Lévy distribution in many-particle quantum systems

A. V. Ponomarev, S. Denisov, and P. Hänggi
Institute of Physics, University of Augsburg, Universitätstrasse 1, D-86159 Augsburg, Germany
(Received 27 July 2009; revised manuscript received 2 October 2009; published 15 April 2010)

The Lévy distribution, previously used to describe complex behavior of classical systems, is shown to characterize that of quantum many-body systems. Using two complimentary approaches, the canonical and grand-canonical formalisms, we discovered that the momentum profile of a Tonks-Girardeau gas—a one-dimensional gas of N impenetrable (hard-core) bosons–harmonically confined on a lattice at finite temperatures obeys a Lévy distribution. Finally, we extend our analysis to different confinement setups and demonstrate that the tunable Lévy distribution properly reproduces momentum profiles in experimentally accessible regions. Our finding allows for calibration of complex many-body quantum states by using a unique scaling exponent.

DOI: 10.1103/PhysRevA.81.043615 PACS number(s): 67.85.−d, 05.30.−d, 05.40.Fb, 47.27.eb

I. INTRODUCTION

Since the first observations of quantum collective phenomena, quantum systems with strongly interacting constituents have become of paramount interest in the condensed matter community [1]. A new wave of activity in the area of quantum many-body systems has been burgeoning with the advent of laser cooling techniques [2]. Many of those quantum models, which were thought to be theoretical abstractions, have since been implemented with cold atoms [3,4]. One such model, a one-dimensional system of hard-core bosons—a Tonks-Girardeau (TG) gas [5]—has been thoroughly probed in recent experiments [6,7].

While the density profile and the energy spectrum of hard-core bosons resemble that of noninteracting fermions, its momentum distribution (MD) exhibits distinct features. The ground state of a homogeneous TG gas is known to possess an infrared divergence in the thermodynamic limit, $N \to \infty$, $n(p) \propto p^{-1/2}$ [8], which, however, vanishes upon addition of a harmonic confinement [9]. So far, there are no analytic results on the infrared behavior of the finite-temperature MD for a finite number of bosons in a harmonic trap. In a sole harmonic confinement, the ground-state MD decays as $n(p) \propto p^{-4}$ in the high-momentum regime [10]. Yet in the presence of an optical lattice, which sets an upper momentum scale given by the recoil momentum, $\hbar k_L$, where k_L is the wave vector of the laser beam, this region cannot be resolved in present state-of-the-art experiments.

The finite-temperature MDs of $N \leqslant 20$ strongly repulsive bosons, confined on a one-dimensional optical lattice and an additional harmonic trap (a "one-dimensional tube"), have been measured experimentally [6]. These measurements revealed that, in the intermediate region, $0.3 \leqslant |p/\hbar k_L| \leqslant 1$, a momentum profile can be approximated by a power law, $n(p) \propto p^{-\gamma}$. The exponent γ depends on temperature, density, and strength of the atom-atom interactions. Results of numerical Monte Carlo simulations have corroborated the experimental finding [11].

What kind of momentum distribution emerges in a system of strongly repulsive bosons? In the present work, we attest that the *Lévy distribution* describes the MD of N thermalized hard-core bosons in various one-dimensional (1d) confinements, in particular, within a single 1d tube as well as within an array of 1d tubes probed experimentally [6,7]. Lévy statistics [12] are known to describe classical chaotic transport [13], processes of subrecoil laser cooling [14], fluctuations of stock market indices [15], time series of single molecule blinking events [16], or bursting activity of small neuronal networks [17]. The appearance of a Lévy distribution in a system output is a strong indicator of a long-range correlation "skeleton" which conducts system intrinsic dynamics [17,18]. However, the Lévy distribution has at no time emerged in the context of *many-particle quantum* systems before. The great advantage of the Lévy-based analysis is its capability of calibration of the TG in different quantum regimes by a unique scaling exponent α.

The paper is organized as follows. In Sec. II, we introduce the lattice TG model and employ two complimentary approaches to study its finite-temperature properties. In Sec. III, we fit exact results of the calculation within the grand-canonical formalism [19] by the Lévy distribution. To provide insight into the experimental situation [6], we devote Sec. IV to the analysis of momentum profiles averaged over the array of 1d tubes. We proceed with the results obtained within the canonical formalism [20] and conclude the section with an analysis of the experimental data from Ref. [6]. In Sec. V, we demonstrate the universality of the Lévy-spline approximation by addressing the MD of a TG gas in one-dimensional confinements of various geometries. We elaborate on the case of a TG gas in a sole harmonic confinement, in a box, and in a sole optical lattice with impenetrable (hard-wall) boundaries. Finally, in Sec. VI, we summarize our results. Some of important technical details are deferred to Appendixes A and B.

II. TONKS-GIRARDEAU GAS AT FINITE TEMPERATURES ON A 1d OPTICAL LATTICE

A Bose gas confined in a deep optical lattice is well described by the Bose-Hubbard Hamiltonian [21]

$$H = -J \sum_l (b_l^\dagger b_{l+1} + \text{H.c.}) + \nu \sum_l l^2 n_l + \frac{U}{2} \sum_l n_l(n_l - 1), \tag{1}$$

where $n_l = b_l^\dagger b_l$ is the particle number operator on lattice site l, J is the hopping strength, the parabolicity $\nu = M\omega_0^2 d^2/2$

is the amplitude of the external harmonic potential with the trapping frequency ω_0, M is the mass of the atom, and d is the lattice constant. The last term in (1) describes the on-site atom-atom interactions. Here we are interested in the TG regime, where the strength of the repulsive atom-atom interaction considerably exceeds the kinetic (hopping) energy, that is, $U/J \to \infty$, [5]. Therefore, the interaction term can be substituted by the condition that two bosons cannot occupy the same lattice site [5].

The momentum distribution can be obtained from the reduced single-particle density matrix $\rho_{n,l}$, reading

$$n(p) = |\Phi(p)|^2 \sum_{n,l} e^{-ip(n-l)} \rho_{n,l}, \qquad (2)$$

where the momentum p is written in units of recoil momentum $\hbar k_L = \pi\hbar/d$, and the envelope $\Phi(p)$ is the Fourier transform of the Wannier function. Note that the latter, as well as the hopping J, is solely defined by the lattice depth, V_0, measured in units of recoil energy, $E_R = (\hbar k_L)^2/2M$.

To find the reduced single-particle density matrix, we employ here the grand-canonical [19] and the canonical formalism [20] (see Appendixes A and B). The first is relevant for a system being in contact with a thermal cloud at constant temperature T, while the second describes an isolated many-particle system.

The difference between the momentum distributions obtained within the grand-canonical and the canonical descriptions is mediated by the number of particles and becomes negligible for $N \gtrsim 10$ [19]. In addition, at finite temperatures $k_B T \gtrsim 0.1J$, systems with different numbers of particles, but the same densities N/n_s, possess the same momentum profiles [19]. Here, $n_s = 8(J\nu)^{1/2}/\pi$ is the number of single-particle eigenstates with nonzero population at the trap center [22]. The latter also yields the critical number of bosons in a 1d tube required to form the Mott insulator in the trap center at zero temperature.

The typical examples of the MD obtained here within the grand-canonical formalism are presented in Fig. 1 for $N \geqslant 10$, where the results of both the grand-canonical and canonical descriptions are practically identical.

III. LÉVY-SPLINE APPROXIMATION

In view of the strong non-Gaussian behavior of the function $n(p)$ [see Fig. 1(c)] and apparent power-law intermediate asymptotics [6,11], it is tempting to compare the MD of a TG gas with a symmetric Lévy distribution [12]. The latter, $L_\alpha(p)$, is a natural generalization of the Gaussian distribution, and it is defined by the Fourier transform of its characteristic function:

$$L_\alpha(p) = \frac{1}{2\pi} \int_{-\infty}^{\infty} \varphi(\xi) e^{ip\xi} d\xi, \quad \varphi(\xi) = \exp(-C_\alpha |\xi|^\alpha), \qquad (3)$$

where the exponent $0 < \alpha \leqslant 2$, and $C_\alpha > 0$ is some constant [12]. For $\alpha = 2$ the distribution is Gaussian. The value of α is invariant under the scaling transformation $p \to \text{const} \cdot p$, which can be used for fitting.

The Lévy distribution exhibits power-law asymptotics, $L_\alpha(p) \propto p^{-(\alpha+1)}$, as $|p| \to \infty$. These "heavy" tails cause the variance of the Lévy distributions to diverge for all $\alpha < 2$.

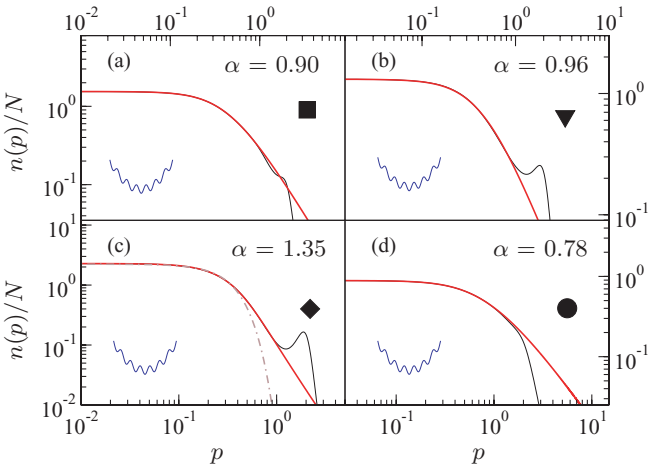

FIG. 1. (Color online) Normalized momentum density profiles for $N = 40$ (a), 30 (b), 10 (c), and 90 (d) hard-core bosons in a 1d tube. The thin (black) lines at four different sets of parameters are compared to Lévy distributions [thick (red) lines]. The dashed-doted line (c) corresponds to a Gaussian approximation. Momentum, p, is measured in units of recoil momentum, $\hbar k_L$. The parameters $(N/n_s, k_B T/J)$ are indicated by the symbols ♦, ▼, ■, and ● in Fig. 2. The thin solid (blue) icon indicates the confinement geometry.

However, this asymptotic limit is not relevant for our objective: The MD for the system (1) is bounded by the width of $|\Phi(p)|$, $(V_0/E_R)^{1/4}\hbar k_L$ [11], so that the MD variance remains finite.

The fitting of the calculated MD $n(p)$ by the Lévy distribution $L_\alpha(p)$ was automatized and performed numerically by the global minimum search of the root-mean-square deviation, $\Delta = \{\sum_j [n(p_j) - L_\alpha(p_j)]^2\}^{1/2}/n(0)$, in a two-dimensional (2d) parametric space $\{\alpha, C_\alpha\}$ (3). For the results shown on Figs. 1 and 2, we took 50 spline points equally spaced on the interval $p \in (0, \hbar k_L)$. The initial area, $\alpha \in (0, 2)$, $C_\alpha \in (0, 30)$,

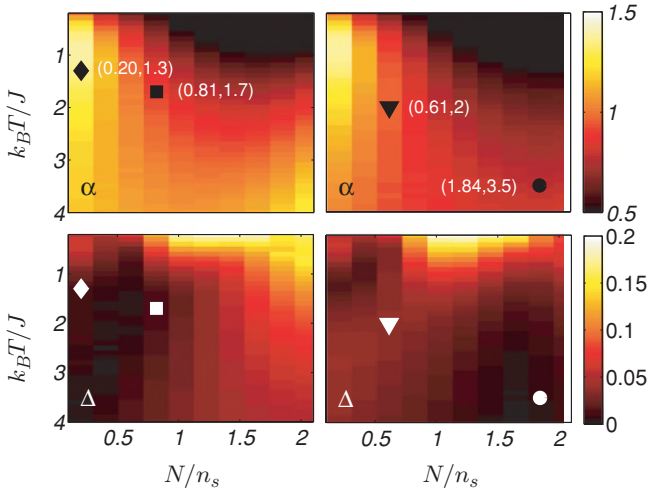

FIG. 2. (Color online) The scaling exponent of the Lévy distribution, α (top), and the corresponding root-mean-square deviation from the exact momentum density profile, Δ (bottom), of TG gas as a function of temperature and particle density for two different amplitudes of the optical lattice, $V_0 = 4.6E_R$ (left column) and $V_0 = 9.3E_R$ (right column) (see text for more details). The amplitude of harmonic confinement is chosen as $\nu = 2 \times 10^{-4} E_R$.

covered by a 10×10 grid was iteratively converged to the global minimum by decreasing the grid step in α and C_α until the desired relative accuracy (fixed to 1% in all figures) was reached.

In Fig. 2, we show the dependence of scaling exponent α (top) on the scaled temperature $k_B T/J$ and the scaled particle density, N/n_s (obtained for $N = 10, \ldots, 100$, and $n_s = 48.78$), together with the associated mean-square deviation Δ (bottom), at relatively low (left) and high (right) amplitude of the optical lattice. These diagrams (see also Fig. 1, for concrete examples of the MD and their Lévy-spline approximations) constitute the first main result of this work, namely, the convergence of the MD of a TG gas toward the Lévy distribution with increasing temperature.

Despite the infinitely strong on-site repulsive interactions, the systematic increase of the Lévy exponent α with temperature [cf. Fig. 2 (top)] is consistent with the high-temperature limit where the ideal Bose gas obeys the classical Boltzmann-Maxwell statistics with a Gaussian MD (i.e., $\alpha = 2$).

IV. AVERAGING OVER THE ARRAY OF 1d OPTICAL LATTICES

The single 1d tube realization, using a fixed temperature T and a fixed particle number N, is not directly accessible with present state-of-the-art experiments. The averaging over an array of tubes done in Ref. [6] can be understood as an averaging over many realizations, with different parameters T and N.

Namely, the experimental setup [6] produces an array of independent 1d tubes, with different numbers of particles, N_i. The probability of having a tube with N particles is given by [6]

$$\varrho(N) = \frac{2}{3}\frac{1}{N_c^{2/3} N^{1/3}}, \quad N \leqslant N_c, \tag{4}$$

where the number of particles in a central tube N_c is a unique parameter. Assuming the same initial temperature in all the tubes for a shallow 1d lattice potential, V_{in}, one can obtain the temperatures at the experimentally adjusted lattice depth, V_0, by using the conservation of entropy in each tube during the subsequent adiabatic increase of the lattice depth from V_{in} to V_0. Therefore, tubes with the different numbers of particles, N_i, acquire different final temperatures, T_i, at $V_0 > V_{\text{in}}$ [6].

We implemented this averaging procedure with $N_c = 18$, for a set of individual MDs precalculated within the canonical formalism. The result for $k_B T = 0.5J$, $V_0 = V_{\text{in}} = 4.6 E_R$, and $\nu = 8 \times 10^{-4} E_R$ is depicted in Fig. 3.

Surprisingly enough, the averaged MD can be perfectly approximated by the Lévy distribution with an "average" scaling exponent, $\tilde{\alpha}$; this is so despite the sizable dispersion of α values appearing in the different momentum profiles.

Therefore, the averaged momentum profile appears as a superposition of several different profiles. It is known that using a proper weight function, $f(\beta)$, one can construct a Lévy distribution from a parametrized set of Gaussian distributions of different dispersion, $L_\alpha(p) = \int_{-\infty}^{\infty} G(p, \beta) f(\beta) d\beta$ [24]. However, we are not aware of any results concerning the superposition of many different Lévy distribution functions with *different exponents* α.

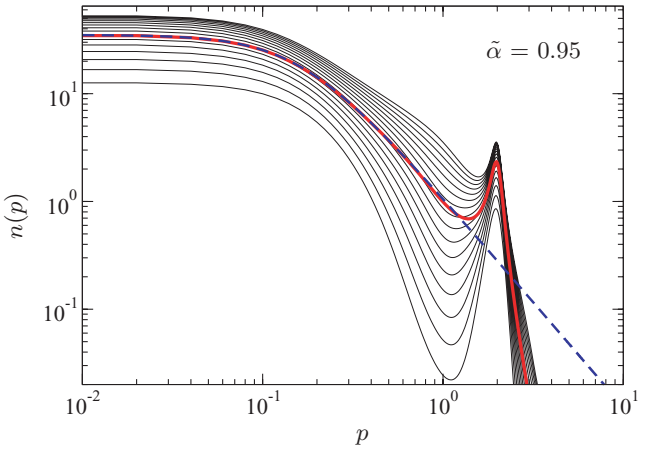

FIG. 3. (Color online) The thin (black) lines are unnormalized momentum distributions for $N = 3, \ldots, 18$ hard-core bosons obtained within the canonical approach (B1). The thick (red) line is the MD averaged over the array of 1d tubes according to the experimental procedure used in Ref. [6] and its best Lévy spline is shown by the thick (blue) dashed line. Momentum, p, is measured in units of recoil momentum, $\hbar k_L$.

A next objective is the comparison of our scheme with the experimental data from Ref. [6] (see Fig. 4). As one can deduce the Lévy distribution yields an excellent approximation for the MD of the experimental system although the latter does not map precisely to a TG gas but rather corresponds to a set of N soft-core bosons with $U/J < \infty$ (1) [11]. In the experiment, one used a power-law fit, $n(p) \propto p^{-\gamma_{\text{exp}}}$, on an intermediate range ($0.3 \leqslant |p/\hbar k_L| \leqslant 1$) [6], with $\gamma_{\text{exp}} - 1 = 1.2, 0.9, 0.4$, and 0.2 for the data shown on Figs. 4(a)–4(d), respectively. We emphasize, however, that in the experimentally accessible region, $|p| \lesssim \hbar k_L$, the power-law behavior with the exponent $\gamma_{\text{exp}} - 1 = \tilde{\alpha}$ of the Lévy distribution is not yet valid, but it is assumed to be only for much larger momentum values. Therefore, the theoretical estimates $\tilde{\alpha}$ in Fig. 4 exceed those

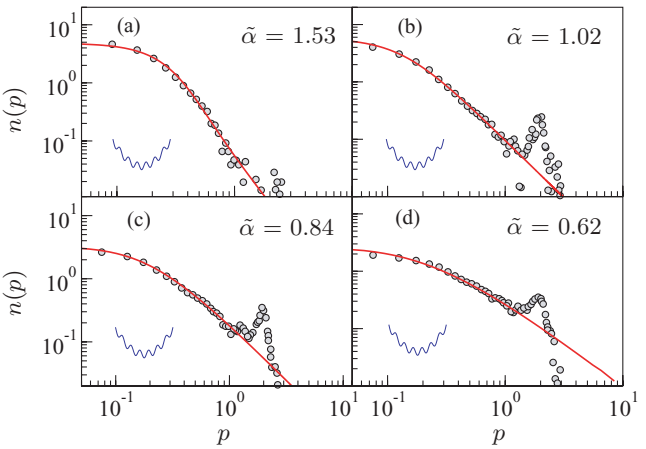

FIG. 4. (Color online) Gray dots are the experimental data for the MD of the 1d quantum gases for different axial lattice depths [6]. The Lévy distributions with the scaling exponent $\tilde{\alpha}$ are shown by the solid (red) lines. The thin solid (blue) icon indicates the confinement geometry. Momentum, p, is measured in units of recoil momentum, $\hbar k_L$.

intermediate-range power-law fit-values (i.e., one consistently finds that $\tilde{\alpha} > \gamma_{\text{exp}} - 1$).

V. UNIVERSALITY OF THE LÉVY SPLINE FOR A TONKS-GIRARDEAU GAS IN 1d CONFINEMENT POTENTIALS

So far we have been dealing with a TG gas on a lattice with an additional harmonic potential (1), which is the only confinement where the MD of a TG gas was experimentally studied in detail [6]. In the present section, we demonstrate applicability of the Lévy-spline approximation to the numerically obtained MD of hard-core bosons at finite temperatures in various 1d confinements: a sole harmonic trap (Fig. 5), a box [Figs. 6(a) and 6(b)], and a sole optical lattice with impenetrable boundaries [Figs. 6(c) and 6(d)].

A TG gas confined in a general potential, $V(x)$, is described by the sum of the single-particle Hamiltonians,

$$H = \sum_{i=1}^{N} \left(-\frac{\hbar^2}{2M} \frac{\partial^2}{\partial x_i^2} + V(x_i) \right), \tag{5}$$

with the hard-core constraint on the bosonic many-particle wave function: $\Psi(x_1, x_2, \ldots, x_N) = 0$ if $|x_i - x_j| < a$, where x_i is the position of ith particle and a is the 1d hard-core diameter. At low density, hard-core bosons can be approximated by impenetrable point-size particles, so that $a = 0$ [5].

The MD of N hard-core bosons in a box, $V_{\text{box}}(x_i) = 0$ if $0 < x_i < L_{\text{box}}$ and $V_{\text{box}} = \infty$ otherwise, and in a harmonic confinement, $V_{\text{osc}} = m\omega^2 x_i^2/2$, was obtained numerically within the canonical formalism with the help of an efficient method [25] which is detailed in Appendix B2. In the case of a sole lattice potential with L lattice sites, the MD was calculated within the grand-canonical formalism by using the same algorithm that was employed in Sec. IV (see Appendix A).

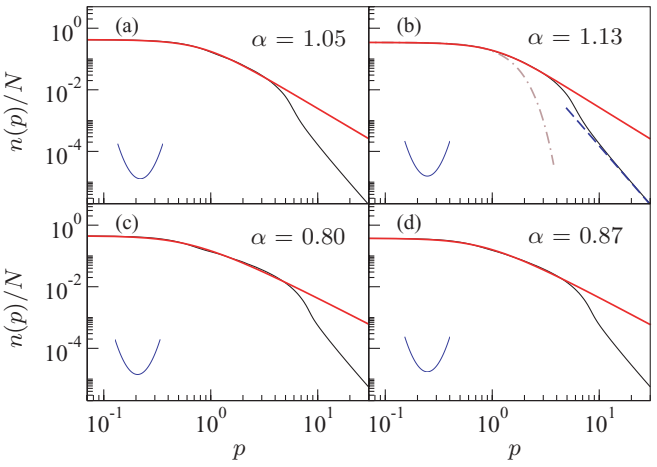

FIG. 5. (Color online) Normalized momentum density profiles for $N = 5$ [(a) and (b)] and $N = 10$ [(c) and (d)] hard-core bosons in a sole 1d harmonic trap. The thin (black) lines, at the two different temperatures $k_B T/\hbar\omega_0 = 1$ [(a) and (c)] and $k_B T/\hbar\omega_0 = 1.5$ [(b) and (d)], are compared to Lévy distributions, shown by the thick (red) lines. Momentum, p, is measured in units of $p_0 = \sqrt{m\hbar\omega_0}$. The dashed line in (b) underlines the well-known universal power-law asymptotic behavior of the Tonks-Girardeau gas momentum distribution at large momenta, p^{-4}, while the dashed-dotted line illustrates the failure of a Gaussian approximation. The thin solid (blue) icon indicates the confinement geometry.

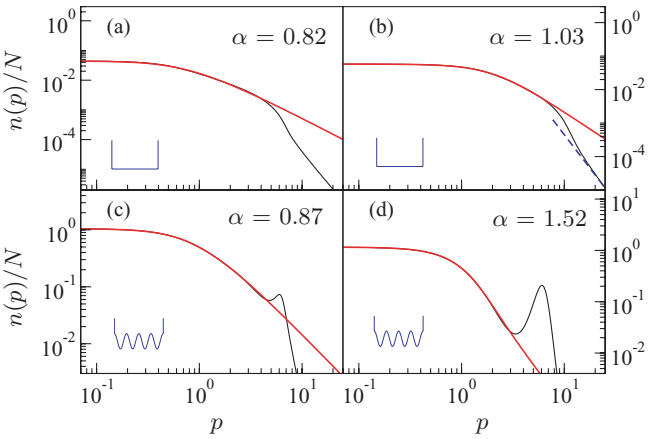

FIG. 6. (Color online) Normalized momentum density profiles for $N = 10$ [(a) and (d)], $N = 5$ (b), and $N = 50$ (c) hard-core bosons in a 1d box [(a) and (b)] of size L_{box} and on a lattice [(c) and (d)] with $L = 100$ lattice sites and the potential amplitudes $V_0 = 4.6E_R$ (c) and $V_0 = 9.3E_R$ (d). The thin (black) lines, at the temperatures $k_B T/\hbar\omega_{\text{box}} = 20$ (a) and 10 (b) and $k_B T/J = 0.5$ [(c) and (d)] are compared to Lévy distributions, shown by thick (red) lines. Here the frequency $\omega_{\text{box}} = \hbar\pi^2/2ML_{\text{box}}$ sets the energy scale, $\hbar\omega_{\text{box}}$, for a particle in a box. Momentum, p, is measured in units of $p_0 = \hbar/L_{\text{box}}$ [(a) and (b)] and $p_0 = \hbar k_L$ [(c) and (d)], in the case of a box and a lattice potential, respectively. The dashed line in (b) underlines the well-known universal power-law asymptotic behavior of the Tonks-Girardeau gas momentum distribution at larger momenta, p^{-4}. The thin solid (blue) icons indicate the two corresponding types of confinement geometry.

It is known, that the MD of a TG gas in a homogeneous toroidal trap and in a harmonic confinement (Fig. 5) exhibits a power-law behavior of p^{-4} for $p \to \infty$ [8]. We also found the same power-law behavior for a TG gas in a box [see Figs. 6(a) and 6(b)]. This in fact turns out to be a general feature of a TG, which also persists at finite temperatures. However, the power-law tail, $p^{-\alpha-1}$, of the Lévy distribution with exponent α cannot decay faster than p^{-3} [12]. Therefore, our Lévy-spline approximation is exclusively aimed at a finite momentum region $(0, p_c)$, where the asymptotic p^{-4} behavior has not yet developed. With Figs. 5 and 6, we demonstrate that the MD of a TG gas at finite temperatures in various 1d confinement potentials (thin lines) can be perfectly approximated by Lévy splines (thick lines) over a significant momentum range.

While at zero temperature we detect a notable deviation of the Lévy spline from the actual MD, with increasing temperature the deviation becomes practically negligible. The exponent of Lévy splines for a TG gas in the confinement potentials presented here depends, in general, on the confinement characteristics, on the gas temperature, and on the particle number or the filling factor, N/L (in the case of a lattice). A more detailed analysis of this dependence will be addressed elsewhere.

VI. CONCLUSIONS

We have presented a study of the finite-temperature momentum distribution of Tonks-Girardeau gases confined in various

1d confinement potentials. The MD of a TG gas on an optical lattice with a superimposed harmonic confinement depends on the particle density, on the lattice depth, and on the gas temperature. We have shown that the tunable Lévy distribution fits momentum profiles up to one recoil momentum with high accuracy. This allows for calibration of TG states with a unique scaling exponent. Thus, our approach completes the attempts to quantify the finite-temperature MDs by using a power-law fitting for the intermediate region $0.3 \leqslant |p/\hbar k_L| \leqslant 1$ [6,11].

We have demonstrated that the MD of a TG gas confined in a 1d box, in a sole 1d harmonic potential, and on a 1d optical lattice with hard-wall boundaries can be approximated by the Lévy distribution function (3) on a finite-momentum region $(0, p_c)$, where for a TG gas the universal power law p^{-4} at large momenta has not yet developed. We thus conjecture that Lévy scaling of MD is a generic feature of a thermalized TG gas.

We want to emphasize one aspect which we consider to be crucial for understanding our approach. It is known that the Lévy distribution has appeared as the stable distribution (i.e., the "attractor" for normalized sums of independent and identically distributed random variables, with no finite mean values). The latter has opened the door to anomalous *statistics* [12]. In our approach, we employ the Lévy distribution (3) merely as a *mathematical function*, which is a natural generalization of the standard Gaussian function, thus leaving aside all the possible statistical interpretations and speculations concerning physical processes responsible for the MD formation. A good example for such "applied" approaches is the widespread use of the Gaussian distribution, which describes the wave function of the ground state of the quantum harmonic oscillator [26] and the Green's function solution of the deterministic heat or diffusion equation [27] and frequently results as a form function in many different physical contexts.

While it is intuitively clear that it is the long-range correlations in the system that cause the emergence of Lévy distributions, the task of unraveling the inherent physical mechanism(s) yielding this anomalous distribution remains a challenge.

ACKNOWLEDGMENTS

We thank an anonymous referee for useful suggestions and comments. This work was supported by the DFG through Grant No. HA1517/31-1 and by the German Excellence Initiative "Nanosystems Initiative Munich (NIM)."

APPENDIX A: GRAND-CANONICAL FORMALISM

Within the grand-canonical description, the number of bosons, N, is a fluctuating quantity and the reduced single-particle density matrix is defined as the trace over the Fock space,

$$\rho_{n,l} = \frac{1}{Z}\mathrm{Tr}\{b_n^\dagger b_l e^{-\beta(H-\mu\sum_j n_j)}\}, \tag{A1}$$

where the chemical potential μ is fixed to give the required number of particles, $N = \sum_l \rho_{l,l}$, in the system, $\beta = 1/k_B T$, with k_B being the Boltzmann factor, and Z is the grand-canonical partition function. The latter coincides with that of noninteracting fermions, that is, $Z = \prod_j [1 + e^{-\beta(\epsilon_j-\mu)}]$, where ϵ_j stands for the single-particle energy spectrum.

The trace over the the Fock space (A1) can be evaluated exactly [19] by mapping the problem of hard-core bosons on that of spinless fermions via the Jordan-Wigner transformation [28]. We next use the expressions for the elements of the reduced single-particle density matrix elaborated in [19], that is,

$$\rho_{n,l} = \frac{1}{Z}\{\det[\mathbf{I} + (\mathbf{I} + \mathbf{A}(n,l))\mathbf{D}(n,l)] - \det[\mathbf{I} + \mathbf{D}(n,l)]\}, \quad \text{for } n \neq l, \tag{A2}$$

$$\mathbf{D}(n,l) = \mathbf{O}(l)\mathbf{U}e^{-(\mathbf{E}-\mu\mathbf{I})/k_B T}\mathbf{U}^\dagger\mathbf{O}(n), \tag{A3}$$

and

$$\rho_{n,n} = [\mathbf{U}(\mathbf{I} + e^{(\mathbf{E}-\mu\mathbf{I})/k_B T})^{-1}\mathbf{U}^\dagger]_{n,n}, \tag{A4}$$

for the main diagonal elements. All operators here are the square matrices $N \times N$ defined as follows: $\mathbf{I}$ denotes the identity matrix, $\mathbf{O}(n)_{i,j} = \{-\delta_{i,j}, i \leqslant n-1; \delta_{i,j}, i > n-1\}$, $\mathbf{A}(n,l)_{i,j} = \delta_{i,n}\delta_{j,l}$, $\mathbf{U}$ is the orthogonal matrix of eigenvectors satisfying the eigenproblem $H_1\mathbf{U} = \mathbf{U}\mathbf{E}$, with the single-particle version of the Hamiltonian (1)

$$H_1 = -J\sum_l (|l+1\rangle\langle l| + \mathrm{H.c.}) + \nu\sum_l l^2 |l\rangle\langle l|, \tag{A5}$$

and $\mathbf{E}$ is diagonal matrix of its eigenvalues (i.e., $\mathbf{E}_{i,j} = \varepsilon_i\delta_{i,j}$). Thus, to obtain the entire matrix $\rho_{n,l}$ ($\rho_{l,n} = \rho_{n,l}^*$) one has to compute $N(N-1)/2$ determinants of $N \times N$ matrices.

APPENDIX B: CANONICAL FORMALISM

In the canonical formalism, the particle reservoir is absent, meaning that one has to find the number, $\mathcal{N}_e$, self-consistently from those many particle states, $|\Psi^m\rangle$, together with their eigenenergies, E_m, that contribute to the thermal superposition at a given temperature. The reduced single-particle density matrix is then obtained as a sum of thermally weighted density matrices, ρ^m, evaluated for each from $\mathcal{N}_e$ eigenstates separately; that is,

$$\rho = \frac{1}{\mathcal{Z}}\sum_{m=1}^{\mathcal{N}_e} e^{-\beta E_m}\rho^m. \tag{B1}$$

The canonical partition function $\mathcal{Z}$ is expressed through the true many-particle energy spectrum: $\mathcal{Z} = \sum_{m=1}^{\mathcal{N}_e} e^{-\beta E_m}$.

The energy spectrum of hard-core bosons is the same as that for spinless fermions: $E_m = \sum_{n=1}^{N} \epsilon_{\alpha_n^m}$, where α_n^m denotes the numbers of single-particle eigenlevels occupied in the mth many-particle state.

1. Hard-core bosons on a lattice

In the case of a lattice confinement, $\rho^m \equiv \rho_{n,l}^m = \langle\Psi^m|b_n^\dagger b_l|\Psi^m\rangle$. The corresponding many-particle eigenstates can be represented as

$$|\Psi^m\rangle = \prod_{\alpha_n^m}\sum_l \mathbf{U}_{l,\alpha_n^m} b_l^\dagger|0\rangle, \quad n = 1, \ldots, N, \tag{B2}$$

where $\mathbf{U}$ is the complete orthogonal set of single-particle eigenvectors (see Appendix A).

Each contribution, $\rho^m_{i,j}$, is related to the Green's function, $G^m_{i,j} = \langle \Psi^m | b_i b_j^\dagger | \Psi^m \rangle$, as

$$\rho^m_{i,j} = G^m_{i,j} + \delta_{i,j}\left(1 - 2G^m_{i,j}\right). \tag{B3}$$

By using the Jordan-Wigner transformation [28], the bosonic Green's function can be rewritten as a scaler product of two fermionic wave functions and subsequently as a determinant of a matrix product [20]:

$$G^m_{i,j} = \det[(\mathbf{P}_m(i))^\dagger \mathbf{P}_m(j)], \tag{B4}$$

where the matrix $\mathbf{P}_m(i)_{l,n}$ has $N+1$ columns:

$$\mathbf{P}_m(i)_{l,n} = \begin{cases} -\mathbf{U}_{l,\alpha^m_n}, & \text{for } l \leqslant i-1, n = 1,\ldots,N; \\ \mathbf{U}_{l,\alpha^m_n}, & \text{for } l > i-1, n = 1,\ldots,N; \\ \delta_{i,l}, & \text{for } n = N+1. \end{cases} \tag{B5}$$

In comparison to the grand-canonical approach, the number of operations needed to obtain the entire matrix $\rho_{i,j}$ is a factor of $\mathcal{N}_e$ larger and is growing with increasing temperature.

2. Hard-core bosons in an arbitrary confinement potential

We have just detailed the canonical formalism for hard-core bosons on a lattice. Now, instead, we elaborate on a general case with arbitrary confinement, $V(x)$. In this case, the momentum distribution, $n(p)$, can be obtained from the reduced single-particle density matrix in the continuum: $n(p) = (2\pi)^{-1}\int dxdy e^{-ip(x-y)/\hbar}\rho(x,y)$, where $\rho(x,y)$ is given by the thermal superposition (B1) with $\rho^m \equiv \rho^m(x,y)$ defined in the following.

To calculate the reduced single-particle density matrix, $\rho^m(x,y)$, in the continuum we make use of an efficient method [25] which represents it in terms of the single-particle states:

$$\rho^m(x,y) = \sum_{i,j=1}^{N} \psi^*_{\alpha^m_i}(x) A^m(x,y)_{i,j} \psi_{\alpha^m_j}(y), \tag{B6}$$

where the $N \times N$ matrix $\mathbf{A}^m(x,y)$ associated with the mth many-particle state is

$$A^m(x,y)_{i,j} = (-1)^{i+j} \det \mathbf{Q}_m(i,j). \tag{B7}$$

$\mathbf{Q}_m(i,j)$ is a minor of matrix $\mathbf{Q}_m$ obtained by crossing the ith row with the jth column, and matrix $\mathbf{Q}_m$ itself is given as

$$Q_m(x,y)_{i,j} = \delta_{i,j} - 2\int_x^y dx' \psi^*_{\alpha^m_i}(x')\psi_{\alpha^m_j}(x'), \tag{B8}$$

where $\psi_n(x)$ are the eigenfunctions of single-particle eigenproblem in a given trapping potential $V(x)$. In (B8), it is assumed that $x \geqslant y$, while for $x \leqslant y$, $\rho^m(x,y) = \rho^m(y,x)^*$. The set of α^m_i, as before in Appendix B1, denotes the numbers of single-particle eigenlevels occupied in the mth many-particle state. Additionally, whenever $\det \mathbf{Q}_m \neq 0$, (B7) can be represented as $\mathbf{A}^m = (\mathbf{Q}_m^{-1})^T \det \mathbf{Q}_m$ [25], which is more efficient when implemented numerically.

For a box and for a harmonic confinement, $\psi_n(x) = \sqrt{2/L_{\text{box}}}\sin(n\pi x/L_{\text{box}})$ and $\psi_n(x) = \sqrt{1/2^n n!}(m\omega_0/\pi\hbar)^{1/4}\exp(-m\omega_0 x^2/2\hbar)H_n(\sqrt{m\omega_0/\hbar}x)$, respectively, where $H_n(y)$ are the Hermite polynomials. For these confinements, the integral in (B8) and the density matrices $\rho^m(x,y)$ can be obtained analytically for a small number of particles with the help of symbolic computational routines. However, expanding out m times N^2 determinants of $(N-1)\times(N-1)$ matrices for $N \gtrsim 5$ quickly becomes unwieldy. Therefore, in Sec. V, the reduced density matrices $\rho^m(x,y)$ were calculated on a numerical grid. The grid step was sufficiently small to ensure a smooth representation of all single-particle wave functions, $\psi_m(x)$, participating in excited many-particle states at a given temperature.

[1] D. J. Thouless, *The Quantum Mechanics of Many-Body Systems* (Academic Press, New York, 1961); A. L. Fetter and J. D. Walecka, *Quantum Theory of Many-Particle Systems* (Dover, New York, 2003).

[2] H. J. Metcalf and P. van der Straten, *Laser Cooling and Trapping* (Springer, New York, 1999).

[3] O. Morsch and M. Oberthaler, Rev. Mod. Phys. **78**, 179 (2006).

[4] I. Bloch, J. Dalibard, and W. Zwerger, Rev. Mod. Phys. **80**, 885 (2008).

[5] M. Girardeau, J. Math. Phys. **1**, 516 (1960).

[6] B. Paredes *et al.*, Nature (London) **429**, 277 (2004).

[7] T. Kinoshita, T. Wenger, and D. S. Weiss, Science **305**, 1125 (2004).

[8] M. Olshanii and V. Dunjko, Phys. Rev. Lett. **91**, 090401 (2003).

[9] T. Papenbrock, Phys. Rev. A **67**, 041601(R) (2003).

[10] A. Minguzzi, P. Vignolo, and M. P. Tosi, Phys. Lett. A **294**, 222 (2002).

[11] L. Pollet, S. M. A. Rombouts, and P. J. H. Denteneer, Phys. Rev. Lett. **93**, 210401 (2004).

[12] W. Feller, *An Introduction to Probability Theory and Its Applications* (Wiley, New York, 1991), Vol. 2.

[13] M. F. Shlesinger, G. M. Zaslavsky, and J. Klafter, Nature (London) **363**, 31 (1993); A. Blumen, G. Zumofen, and J. Klafter, Phys. Rev. A **40**, 3964 (1989).

[14] F. Bardou, J.-P. Bouchaud, A. Aspect, and C. Cohen-Tannoudji, *Levy Statistics and Laser Cooling* (Cambridge University Press, Cambridge, 2002).

[15] R. N. Mantegna and H. E. Stanley, Nature (London) **376**, 46 (1995).

[16] E. Barkai, R. Silbey, and G. Zumofen, Phys. Rev. Lett. **84**, 5339 (2000).

[17] R. Segev, M. Benveniste, E. Hulata, N. Cohen, A. Palevski, E. Kapon, Y. Shapira, and E. Ben-Jacob, Phys. Rev. Lett. **88**, 118102 (2002).

[18] C.-K. Peng, J. Mietus, J. M. Hausdorff, S. Havlin, H. E. Stanley, and A. L. Goldberger, Phys. Rev. Lett. **70**, 1343 (1993).

[19] M. Rigol, Phys. Rev. A **72**, 063607 (2005).

[20] M. Rigol and A. Muramatsu, Phys. Rev. A **70**, 031603(R) (2004); **72**, 013604 (2005).

[21] D. Jaksch, C. Bruder, J. I. Cirac, C. W. Gardiner, and P. Zoller, Phys. Rev. Lett. **81**, 3108 (1998).
[22] The critical density n_s is found via mapping the single-particle version of (1) onto the quantum pendulum [23].
[23] A. V. Ponomarev and A. R. Kolovsky, Laser Phys. **16**, 367 (2006).
[24] C. Beck and E. G. D. Cohen, Physica A **322**, 267 (2003).
[25] R. Pezer and H. Buljan, Phys. Rev. Lett. **98**, 240403 (2007).
[26] R. L. Liboff, *Introductory Quantum Mechanics* (Addison-Wesley, San Francisco, 2003).
[27] G. Barton, *Elements of Green's Functions and Propagation* (Oxford University Press, Oxford, 1989).
[28] P. Jordan and E. Wigner, Z. Phys. **47**, 631 (1928).